SCIENCE CHINA
Earth Sciences

SPECIAL TOPIC: Water in the Earth's interior
•REVIEW•

April 2016 Vol.59 No.4: 696–706
doi: 10.1007/s11430-015-5249-5

Experimental study of the electrical conductivity of hydrous minerals in the crust and the mantle under high pressure and high temperature

GUO XinZhuan*

State Key Laboratory of Geological Process and Mineral Resources, China University of Geosciences, Wuhan 430074, China

Received August 6, 2015; accepted December 2, 2015; published online February 18, 2016

Abstract Hydrous minerals are important water carriers in the crust and the mantle, especially in the subduction zone. With the recent development of the experimental technique, studies of the electrical conductivity of hydrous silicate minerals under controlled temperature, pressure and oxygen fugacity, have helped to constrain the water distribution in the Earth's interior. This paper introduces high pressure and temperature experimental study of electrical conductivity measurement of hydrous minerals such as serpentine, talc, brucite, phase A, super hydrous phase B and phase D, and assesses the data quality of the above minerals. The dehydration effect and the pressure effect on the bulk conductivity of the hydrous minerals are specifically emphasized. The conduction mechanism of hydrous minerals and the electrical structure of the subduction zone are discussed based on the available conductivity data. Finally, the potential research fields of the electrical conductivity of hydrous minerals is presented.

Keywords Electrical conductivity, High pressure and temperature experiment, Hydrous minerals, Conduction mechanism, Subduction zone, High conductivity anomalies

Citation: Guo X Z. 2016. Experimental study of the electrical conductivity of hydrous minerals in the crust and the mantle under high pressure and high temperature. Science China Earth Sciences, 59: 696–706, doi: 10.1007/s11430-015-5249-5

1. Introduction

In the subduction zone, hydrous minerals in the crust and the mantle are the main water carriers. The hydrous minerals can be carried into the Earth's deep interior even up to the top of the lower mantle if the subduction is characterized by low geotherm, high angle and high speed. Water derived from the dehydration of the hydrous minerals in the slab will move upwards and significantly influence the physical and chemical properties of the minerals and the dynamic process in the Earth (Winkler and Nur, 1982; Meade and Jeanloz, 1991; Pawley and Holloway, 1993; Mei and Kohlstedt, 2000; Nishihara et al., 2006; Karato, 1990).

Electrical conductivity of the hydrous minerals is controlled by temperature, pressure, crystal structure, and preferred orientation of the hydrous minerals. However, electrical conductivity of the hydrous minerals is independent of the water content in the minerals (Guo and Yoshino, 2013). This is very different from the nominally anhydrous minerals in which a small amount of water adopted in the structure can significantly enhance the electrical conductivity (Karato, 1990).

Experimental study of the electrical conductivity of hydrous minerals under high pressure and temperature combined with magnetotelluric data can directly constrain the compositional structure, properties and distribution of water in the Earth's interior. With the continuous advancements of

*Corresponding author (email: gxzhuan@cug.edu.cn)

the high-pressure and high-temperature apparatus and the experimental technique over the last decade, the experimental study of the electrical conductivity of hydrous minerals has made rapid progress, and becomes a new hot issue in the field of the Earth science. The relevant research has broadened the understanding of the conducting mechanism of the hydrous minerals and also enriched our knowledge of the water distribution in the Earth's interior. Based on the recent progress, this paper introduces the state of the art experimental method to measure the electrical conductivity of hydrous minerals (emphasizing the special notes during the experiments), assesses the validity of the experimental data, identifies the various influencing factors, and describes the conduction mechanism in detail. Finally the electrical structure of the subduction zone is discussed.

2. Conductivity measurements of the hydrous minerals under high pressure and temperature

Yoshino (2010) and Yang (2014) already summarized the basic principle and methods of the conductivity measurements of the minerals, which will not be detailed here. Impedance spectroscopy technique acquired in a wide frequency range is widely accepted now. The measurements using direct current (Hinze et al., 1981) and low frequency methods (Yoshino et al., 2006, 2008; Katsura et al., 1998) are no longer adopted (see Yang (2014)). As impedance spectroscopy technique can well identify different conduction mechanisms, this method is widely used in measuring the conductivity of solid samples (including monocrystal and polycrystal samples), fluid-solid samples, and fluid phase samples. Conductivity measurements of the hydrous minerals also adopt this method.

It is very important to choose suitable temperature, pressure and the sample container for the conductivity measurement of hydrous minerals . The stability field of the hydrous mineral is narrow relative to that of the nominally anhydrous minerals (NAMs). To obtain the real conductivity data of the sample itself, we should therefore preclude the influences of dehydration and partial dehydration of the hydrous minerals (see the discussions below) on the conductivity measurements. Hydrous minerals easily react with the sample container to produce water, which will invalid the conductivity measurement of the hydrous minerals themselves. Guo et al. (2011) measured the conductivities of the natural serpentinites and talc rocks. They initially used MgO as the sample container, which reacted with talc sample even at low temperatures. The reaction products, enstatite and water, greatly enhanced the bulk conductivities and made the measurement invalid. Later Al_2O_3 container was used and the dehydration reaction no longer occurred, guaranteeing the data quality. After the conductivity measurements, it is necessary to check the reaction between the container and the sample using the secondary electron scanning microscope. If the reaction rim is observed, the sample may have dehydrated and as even small amount of water will influence the measurement validity, we should change suitable material as the sample container or decrease the experimental temperature to avoid the dehydration of the sample.

3. Electrical conductivity of hydrous minerals under high pressure and temperature

Until now electrical conductivities of the hydrous minerals, including serpentine, talc, brucite, and dense hydrous magnesium silicate (DHMS: phase A, super hydrous phase B and phase D), have been measured in detail. Hydrous minerals act like an insulator at room temperature. However, they behave as semiconductors at high temperatures. The relationship between conductivity (σ) and temperature (T) can be expressed by Arrhenius function:

$$\sigma = \sigma_0 \cdot \exp\left(\frac{\Delta H}{kT}\right), \quad (1)$$

where σ_0 is the pre-exponent factor, ΔH is the activation enthalpy, k is the Boltzmann constant, and T is the absolute temperature. Electrical conductivities of different hydrous minerals under high pressure and temperature will be shown in the following sections.

3.1 Electrical conductivity of serpentine

Figure 1 shows the conductivity measurement of serpentines under high pressure and temperature. Guo et al. (2011)

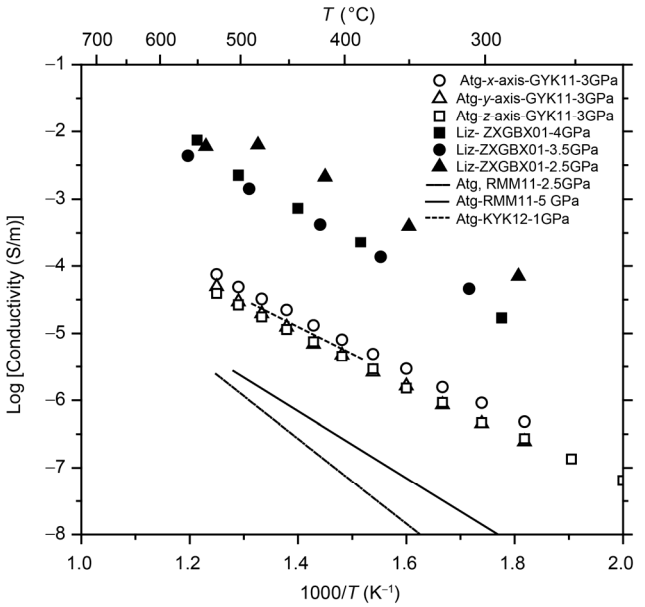

Figure 1 Electrical conductivity of serpentine as a function of reciprocal temperature. Atg, antigorite; Liz, lizardite; ZXGBX01, Zhu et al. (2001a); RMM11, Reynard et al. (2011); KYK12, Kawano et al. (2012).

measured the electrical conductivity of natural deformed serpentinites (major mineral is antigorite). Their results show that the highest conductivity of antigorite (along the lineation of the sample) is about 1 to 2 orders of magnitude lower than the conductivity of polycrystalline lizardite (Zhu et al., 2001a). This difference might be caused by: (1) the different starting materials. (2) Zhu et al. (2001a) used the dehydrated pyrophyllite as the sample container. However, the dehydration products of pyrophyllite, Al_2SiO_5 and SiO_2, would have reacted with the serpentine sample to produce water, which influenced the validity of the measurement. This possible dehydration reaction was not carefully checked and described in their paper. (3) Reynard et al. (2011) argued that the impedance arcs in the experiments of Zhu et al. (2001a) missed the origin and the conductivity value tends towards the values obtained in the short-circuited runs in their experiments. Except the enormous difference of the absolute conductivity values between Zhu et al. (2001a) and Reynard et al. (2011), the pressure effect on the conductivity of serpentine in their experiments is opposite.

The conductivity values of antigorite obtained by Reynard et al. (2011) are 1 order of magnitude lower than Guo et al. (2011). It was difficult to explain the discrepancy between their studies because the experimental conditions were similar and they both used Al_2O_3 as the sample containers. One possible reason might be the orientation of antigorite in the sample of Guo et al. (2011). The conductivities of Fe-free polycrystalline serpentine at 1 GPa reported by Kawano et al. (2012) are consistent with those of Guo et al. (2011).

Guo et al. (2011) showed that: (1) the orientation of antigorite in serpentinite caused an electrical conductivity anisotropy (defined as $\sigma_{max}/\sigma_{min}$, the maximum difference between $\log\sigma_{max}$ and $\log\sigma_{min}$ is around 0.5); (2) the conductivities along the lineation and perpendicular to the foliation were highest and lowest, respectively; (3) the activation enthalpy of serpentine was between 0.59 and 0.69, supporting proton conduction as the dominant conduction mechanism. In addition, electrical conductivity of serpentine buffered by Ni-NiO was about 0.25 order of magnitude higher than that buffered by Mo-MoO_2. When Ni-NiO buffer was used, more vacancies formed in the hydrogen position due to the reaction (V'_H): $\frac{1}{2}O_2 + Fe^X_{Mg} = Fe^2_{Mg} + V'_H + O^X_O$, providing more paths for proton migration. As a result, the bulk conductivity increased. Moreover, Guo et al. (2011) showed that the conductivities of experiments buffered by Mo-MoO_2 and Ni-NiO electrodes were consistent with those using Mo and Ni metal electrodes, respectively. This result suggests that the oxygen fugacity of the serpentinite samples have been controlled by the Mo-MoO_2 and Ni-NiO buffers even if Mo and Ni metal electrodes have been used.

Kurtz et al. (1986) reported that in the Juan de Fuca subduction zone there was a high conductivity layer ($10^{-1.5}$ S/m) along the slab (shearing direction) at depth of 15–60 km. Based on deformation experiments, Katayama et al. (2009) concluded that the orientation of the serpentine (serpentinization of olivine) in the upper mantle was normal to the subducting slab, which would cause the strong anisotropy of the seismic velocity. Therefore one may wonder if high conductivity layer in the Juan de Fuca subduction zone could result from the orientation of the serpentine minerals. According to experiments of Guo et al. (2011) the highest conductivity value is $10^{-4.1}$–$10^{-3.6}$ S/m (T: 720–870 K, neglecting the pressure effect). Therefore, the orientation of serpentine minerals cannot explain the high conductivity layer in the Juan de Fuca subduction zone. It also cannot explain the high conductivity anomalies ($10^{-1.5}$ S/m, Wannamaker et al., 2009) observed in the New Zealand subduction zone .

There likely are other high conductive phases in the mantle wedge where high conductivity anomalies exist, e.g., interconnected phases of magnetite or saline. Kawano et al. (2012) measured the electrical conductivity of magnetite-bearing serpentinites under shear deformation. They found that 25 vol% of magnetite was needed to establish its interconnection even with shear strain up to 9. However, the magnetite fraction is commonly less than 5 vol% in natural serpentinites, therefore the high conductivity anomalies cannot be explained by the magnetite-bearing serpentinites during shear deformation at the plate interface in the mantle wedge. Reynard et al. (2011) suggested that the geophysical observation of 1 S/m conductivity anomaly could be explained by the serpentinites with 1 vol% saline (molality of 3 mol/kg) according to the calibration.

3.2 Electrical conductivity of talc

Talc is a common hydrous mineral in the crust. Two common parageneses are: (1) low-grade metamorphism (and hydrothermal alteration) of ultrabasic rocks; (2) contact and regional metamorphism of siliceous dolomites. In ultrabasic rocks the talc is commonly accompanied by serpentine and olivine in lenticular veins. Metasomatism with high Si activity favours the formation of talc.

Figure 2 shows the electrical conductivity of talc under high pressure and temperature. Zhu et al. (2001b) reported the electrical conductivity of natural talc at 1 and 2 GPa. They found that the electrical conductivity of talc did not change abruptly when dehydration occurred, with the activation enthalpy as high as 2.5 eV. The activation enthalpy of talc reported by Guo et al. (2011) was between 0.59 and 0.67 eV, which was consistent with that (0.52 eV) of Wang and Karato (2013). The activation enthalpy of 2.5 eV represents the ionic conduction mechanism, whereas less than 1 eV represents the proton conduction mechanism. Ionic conduction unlikely dominates the conduction mechanism

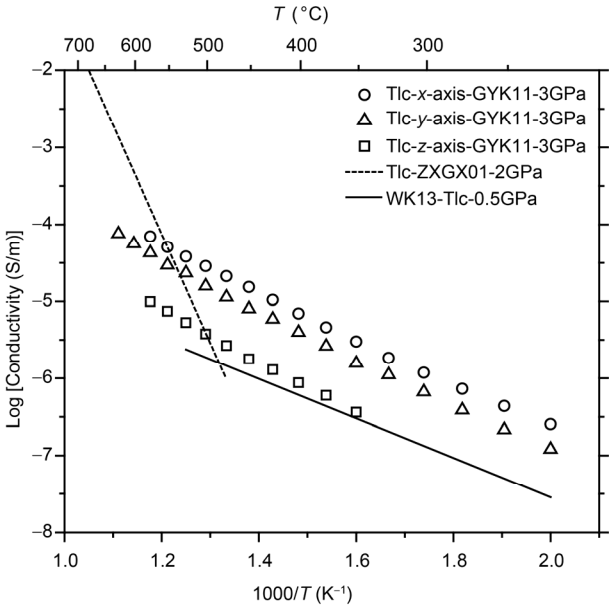

Figure 2 Electrical conductivity of talc under high pressure and temperature. Tlc, talc; GYK11, Guo et al. (2011); ZXGX01, Zhu et al. (2001b); Wk13, Wang and Karato (2013).

when the experimental temperature is less than 900 K. Therefore, the results of Guo et al. (2011) and Wang and Karato (2013) seem to be more reliable.

The orientation of talc mineral caused strong conductivity anisotropy of the talc bearing rock: the highest and lowest conductivity are along the lineation and l perpendicular to the foliation, respectively (Guo et al., 2011). Electrical conductivity is lower in talc than in serpentine, but the conductivity anisotropy of talc is stronger than that of serpentine within their stability fields. Although talc contains a lot of structural water (about 5 wt%), the conductivity is similar to that of olivine containing 177 ppm water (Yoshino et al., 2006). Therefore, the effect of water content on the electrical conductivity of hydrous minerals and nominally anhydrous minerals is completely different. It can be concluded that most protons in talc (also in serpentine) cannot move easily, but are bound in the lattice positions.

3.3 Electrical conductivity of brucite

Brucite serves as the texturally and compositionally simplest hydrous mineral with layered structure. Therefore, it is the best candidate to understand the conduction mechanism of hydrous minerals.

Fuji-ta et al. (2007) measured the electrical conductivity of brucite in the close system at 1 GPa. When dehydration occurred (T: ~700 K) electrical conductivity of brucite rapidly increased and the relationship between the electrical conductivity and the reciprocal temperature no longer satisfied the Arrhenius function. A single-crystal sapphire was used as the sample container in their experiments to prevent water escaping at high temperatures. As a result, the achieved pressure for the sample was far lower than expected, less than 0.5 GPa at 700 K according to the phase diagram. Given that there is a positive effect of pressure under 10 GPa on the electrical conductivity of brucite (see the discussion in section 5 and 6), the results of Fuji-ta et al. (2007) are the ones measured at pressures lower than 1 GPa. Guo and Yoshino (2014) reported the pressure effect on the conductivity of brucite single-crystal. Impedance spectroscopy measurements demonstrated that electrical conductivity perpendicular to the c-axis is nearly half order of magnitude higher than the one parallel to the c-axis under the same P-T conditions. Electrical conductivity was strongly enhanced during the compression of sample to 11 GPa, irrespective of crystallographic direction. However, the conductivity increase with pressure became less significant upon further compression from 11 to 13 GPa.

The experimental data of different studies are consistent under similar P-T conditions. Considering the enormous pressure effect on the electrical conductivity of brucite, those data are not consistent in fact. Moreover, Fuji-ta et al. (2007) continuously increased temperature from room temperature to the dehydration temperature and did not keep the sample at 700 K to preclude the adsorbed moisture from the air. Therefore, the absolute conductivity values of brucite before the dehydration were high (Figure 3).

The results of Gasc et al. (2011) and Guo and Yoshino (2014) are relatively consistent in the low temperature range. But the activation enthalpy of the former is about 0.1–0.2 eV higher than that of the latter.

3.4 Electrical conductivity of the DHMS minerals

DHMS minerals are the important hydrous minerals in the subduction zone. Phase H ($MgSiO_4H_2$), currently the high-

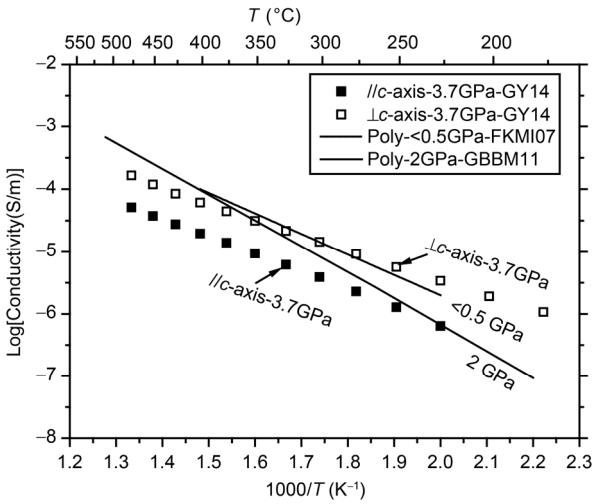

Figure 3 Electrical conductivity of brucite under high pressure and temperature. Poly, polycrystalline; GY14, Guo and Yoshino (2014); FYMI07, Fuji-ta et al. (2007); GBBM11, Gasc et al. (2011).

pressures up to 60 GPa (Nishi et al., 2014; Ohtani et al., est pressure phase of hydrous minerals, can be stable at 2014), suggesting that water can potentially be carried into the lower mantle as deep as 1800 km.

Until now, only Guo and Yoshino (2013) measured the electrical conductivity of phase A at 10 GPa, super hydrous phase B at 18 GPa, and phase D at 22 GPa, respectively, using the Kawai-type multi-anvil press (Figure 4). They initially synthesized the DHMS samples in the sealed Pt capsule and further sintered them again in the unsealed Mo capsule to remove the free water adsorbed in the synthesized sample. This kind of pre-processing can minimize the effect of free water on the bulk conductivity of the sample. Testing experiments showed that there was a good linear relationship between $\log\sigma$ and $1/T$ when temperature was lower than 800 K. However, electrical conductivity increased quickly when temperature approached 800 K due to the dehydration reaction between the sample and the MgO container. The upper limit of the experimental temperature was therefore set at 775 K. Their experimental results show that : (1) the increase of electrical conductivity with temperature follows the Arrhenian function. The activation enthalpies of phase A, super hydrous phase B and phase D yield values of 0.77±0.01, 0.83±0.01 and 0.75±0.01 eV, respectively; (2) the higher pressure DHMS phases shows higher conductivity values. The electrical conductivities of phase D and super hydrous phase B are about two orders and one order of magnitude higher than that of phase A in the same temperature range, respectively. The conductivity of DHMS phase is closely related to the O···O distance (distance between two neighboring O) because the potential barrier for proton migration from the donor OH^{-1} to the accepter O^{2-} decreases with O···O distance. Proton conduction in phase D is the easiest due to the shortest O···O distance among these three phases.

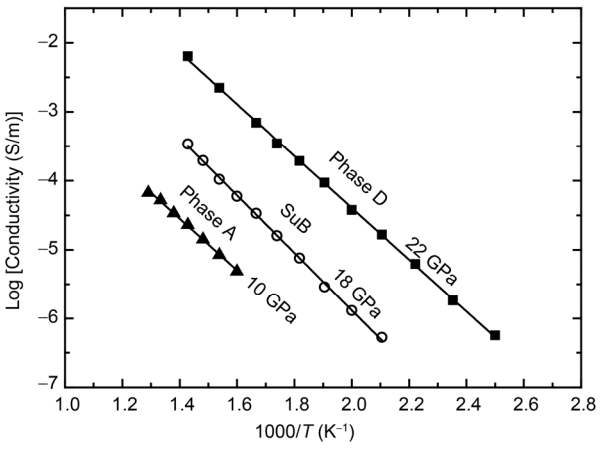

Figure 4 Electrical conductivity of Phase A, super hydrous phase B and phase D as a function of reciprocal temperature, respectively. Figure was modified from Guo and Yoshino (2013).

4. Effect of dehydration on the electrical conductivity of hydrous minerals

Free water will be released through dehydration reaction when the experimental conditions are beyond the stability field of hydrous minerals. Some ionic species dissolved in the free water (e.g., K^+, Na^+, H^+, Mg^{2+}) can significantly enhance the bulk conductivity because of their high mobility. Gasc et al. (2011) performed a representative study about the dehydration effect on the conductivity of brucite . In their experiments, the bulk conductivity increased 6–7 orders of magnitude after the dehydration of brucite. The activation enthalpies are 0.11 and 1.1 eV with and without the grain boundary water, respectively.

In situ monitoring the electrical conductivity under high pressure and temperature is one method to define the stability field of the hydrous minerals (Fuji-ta et al., 2007; Gasc et al., 2011). However, the dehydration temperature inferred from the conductivity change is always inconsistent with that defined by the conventional phase transition experiments. For example, the dehydration temperature of serpentine at 3 GPa indicated by electrical conductivity experiment is 900 K from which electrical conductivity continuously increased (Guo et al., 2011). However, the dehydration temperature defined by phase transition experiment is 980 K (Ulmer and Trommsdorff, 1995). Furthermore, the dehydration temperature of brucite at 2 GPa inferred from the conductivity change is 803 K (Gasc et al., 2011) and it is defined by phase transition experiments at about 1273 K (Schramke et al., 1982). This contradiction may be explained by the facts that the hydrous minerals just partially dehydrate when experimental temperature approaches the dehydration temperature , rather than completely dehydrate. In the case of brucite, the abrupt change of the electrical conductivity represents the escaping of hydrogen from the lattice structure forming high defect crystal structure $Mg(OH)_{2-x}O_{x/2}D_{x/2}$ (D is the Schottky-Frenkel defect couple, $x<2$). However, the crystal structure of brucite (trigonal symmetry) does not collapse immediately to form cubic MgO until most of the protons have escaped. The partially dehydrated sample of brucite was confirmed to be brucite by the micro-focused X-ray diffraction analysis. No periclase peaks have been indexed. Until now, there are no *in situ* infrared spectroscopy studies supporting the partial dehydration process of hydrous minerals except the *in situ* conductivity measurements.

Water will migrate along the grain boundary when it is released from the hydrous minerals, which can be monitored by the impedance spectroscopy. Guo and Yoshino (2013) demonstrated how to detect the free water using the technique of impedance spectroscopy. The impedance spectrum was characterized by two partly overlapped semicircles when super hydrous phase B was heated to 600 K at 18 GPa (Figure 5a), suggesting presence of two RC parallel

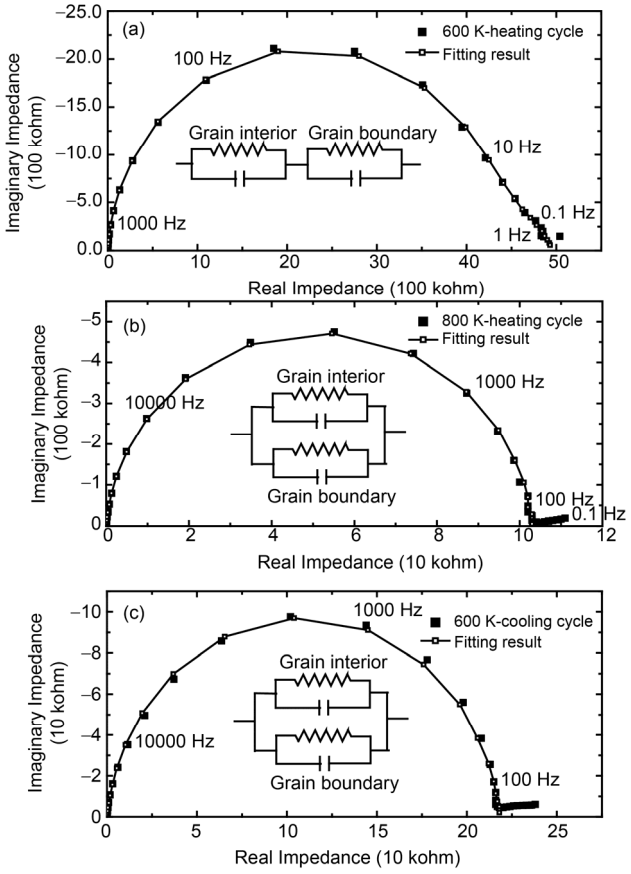

Figure 5 Characterized changes of the impedance spectroscopy of the partially dehydrated hydrous minerals. Modified from Guo and Yoshino (2013).

circuit (R is a resistor, C is a capacitor). When the sample was heated to 800 K, partial dehydration occurred, resulting in a single semicircular shape of impedance spectrum (Figure 5b). The changes of the spectra during heating suggested that the establishment of interconnected free water in the sample. The equivalent circuit is composed of two R-C parallel circuits in parallel. Considering the high mobility of the electric charge carriers in free water, the signal of fluid phase determines the bulk resistance of the dehydrated sample. When the sample was cooled to 600 K, the interconnected pathway of the fluid still remained which was inferred the semicircle-shape spectrum. Meanwhile, the absolute value of the resistance was reduced by 1 order of magnitude (Figure 5c).

The partial dehydration or the complete dehydration of hydrous minerals can both change the water activity of the system and enhance the bulk conductivity. It is challenging to measure the conductivity of the hydrous minerals before and after dehydration occurs in particular due to the difficulty in finding suitable sample container which simultaneously acts as an electric insulator, prevents water escaping and does not react with the sample. Most of the previous experimental studies were conducted in an open system in which water leak are not prevented. The conductivity of the dehydrated sample in the open system continuously changes with time. Until now only the experimental cell of Fuji-ta et al. (2007) provided a close condition. The sapphire sample container was however too hard to generate the expected pressure. Moreover, further factors affect the conductivity of the samples in the close system, e.g., the state of the fluid, the pore pressure and the fluid composition must be considered.

5. Conduction mechanism of the hydrous minerals

The conduction mechanisms of the hydrous minerals with different chemical composition are not unique. For the Fe-free hydrous minerals (e.g., pure brucite), proton conduction is the dominant mechanism. For the Fe-bearing hydrous minerals, the conduction mechanisms include the proton conduction and the small polaron conduction mechanisms. Most hydrous minerals are silicate minerals with layered structure. Brucite serves as the simplest prototype of the hydrous minerals. In order to understand the conduction process on the atomic scale, I will focus on brucite to discuss the proton conduction mechanism.

The crystal structure of brucite is in trigonal symmetry (space group: $P\bar{3}m1$) (Figure 6), which is characterized by: (1) [MgO_6] octahedron layers stack along the *c*-axis; (2) OH dipole orientates along the *c*-axis; (3) repulsive force exists between proton and the nearest neighboring protons. The hydroxyl protons in $Mg(OH)_2$ are tightly bound to the O^{2-} at room temperature, because the ionic radius of O^{2-} (1.33×10^{-10}–1.40×10^{-10} m, Freund and Wengeler, 1980) is longer than O-H distance (0.958×10^{-10} m, Catti et al., 1995). However, some of the hydroxyl protons can be thermally activated when temperature is high enough (e.g., 600 K) through the reaction:

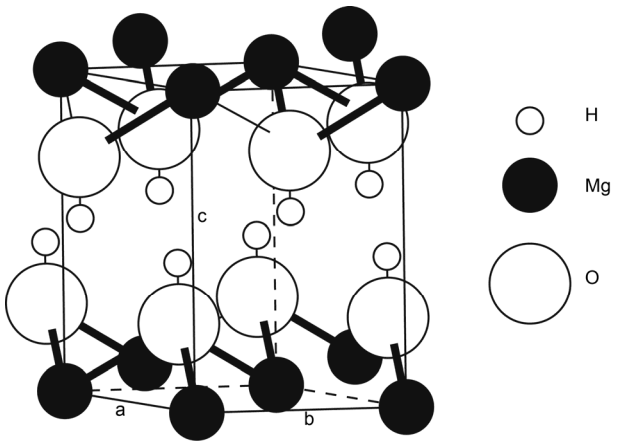

Figure 6 Crystal structure of brucite. perspective view of the $P\bar{3}m1$ structure showing the downward pointing proton surrounded by three upward pointing proton. The protons are in the 2*d* position (1/3, 2/3, Z_H).

$$OH^- + OH^- \Leftrightarrow HOH + O^{2-} \quad (1)$$

where HOH represents the excess proton on the lattice site of -OH, and O^{2-} denotes a vacancy at the H site (chemically, O^{2-}). Once dissociated from its O^{2-} the excess proton at the HOH site can migrate from the origin lattice site to the neighboring hydroxide lattice according to:

$$HOH + OH^- \Leftrightarrow OH^- + HOH \quad (2)$$

It thus becomes an excess proton in the hydroxide lattice. Alternatively, the defect lattice (O^{2-}) also has probability to capture the proton from the neighboring-OH:

$$O^{2-} + OH^- \Leftrightarrow OH^- + O^{2-} \quad (3)$$

Reaction (3) is a hydrogen bond-type exchange process of hydrogen. The hydrogen defects (O^{2-}) include two types: one is generated by the thermally activated process in reaction (1) (the intrinsic mechanism), and the other type is required to compensate for the charge imbalance due to chemical impurities (extrinsic mechanism). Proton conduction may be controlled by reaction (2) and (3).

Guo and Yoshino (2014) and Guo et al. (2013) measured the electrical conductivity of the single crystalline brucite and the diffusivity of hydrogen in the single crystalline brucite, respectively. Based on the conductivity and diffusivity data the ratio of the activated protons contributing to the conduction process under high pressure and temperature can by estimated using the Nernst-Einstein equation. Figure 7 shows the ratio of the free protons over the total protons of the brucite single crystal at 950 K as a function of pressure. The ratio increases with pressure: 2.3–2.5% at 3.7 GPa and 30.1–33.0% at 13 GPa. That is, not all protons contribute to the conduction process under high pressure and temperature. Most of the protons are bound in the normal lattice site, indicating that the conductivity of the hydrous minerals are independent of the total water content, but dependent on the thermally activated protons. The electrical conductivity of the nominally anhydrous minerals (such as wadsleyite) however depends on the water content because the substitution of normal lattice atoms (e.g., Mg^{2+}) by protons will generate vacancies and provide more paths for proton migration.

Some hydrous minerals are only stable at low pressures and temperatures. For instance, the dehydration temperature of antigorite at 3 GPa is 950 K, at which the dominant conduction mechanism is proton conduction rather than small polaron mechanism. Figure 8 shows the electrical conductivities of Fe-bearing (X_{FeO}=7.3 wt%) and basically Fe-free (X_{FeO}=0.1 wt%) antigorite samples. The data of these two samples are quite consistent suggesting that the conductivity of antigorite at temperature below 900 K is independent of Fe concentration. Thus, small polaron conduction mechanism does not play an important role for antigorite at temperature below 900 K, however Fe-bearing phase D and super hydrous phase B can be stable at temperatures up to

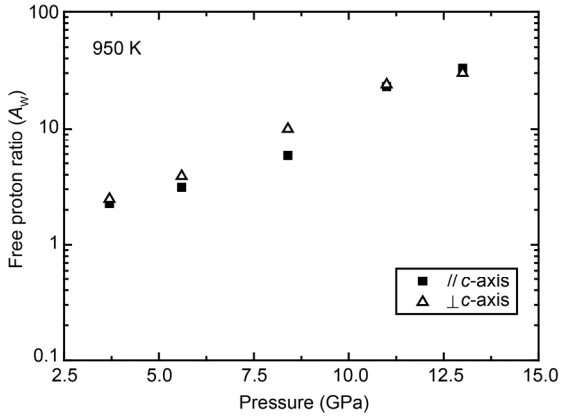

Figure 7 The ratio of free protons over the total protons in the normal lattice sites at 950 K as a function of pressure. Black square and open triangle denote the data along and normal to the *c*-axis, respectively. This figure is modified from Guo and Yoshino (2014).

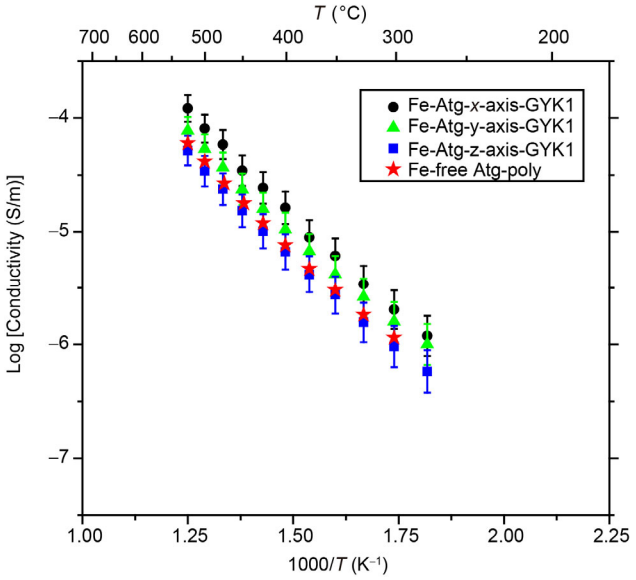

Figure 8 Electrical conductivity of the Fe-bearing and Fe-free antigorite. GYK11, Guo et al. (2011). The vertical bar denotes the error. poly, polycrystalline sample.

1500 K or even more. In this case, we have to consider the contribution of small polaron conduction to the conductivity.

6. Pressure effect on the conductivity of hydrous minerals

For hydrous minerals and NAMs, the relationship between the conductivity, temperature and pressure satisfies:

$$\sigma = \sigma_0 \exp\left(-\frac{\Delta U + P\Delta V}{kT}\right), \quad (2)$$

where ΔU is the activation energy, ΔV is the activation volume, and P is the pressure. However, pressure effects on

these two types of minerals are dependent on the conduction mechanism. Xu et al. (2000) reported the pressure effect on the conductivity of water-free polycrystalline San Carlos olivine ($Mg_{1.8}Fe_{0.2}SiO_4$). The activation volume is 0.6±0.6 cm^3/mole, indicating a negative pressure effect. They explained that lattice distortion under higher pressure will prevent electron hopping between Fe^{2+} and Fe^{3+} and therefore lowered the conductivity. Pressure effect on the conductivity of NAMs is generally small and the pressure effect on the conductivity is usually neglected in calculating the conductivity-depth profile (Huang et al., 2005; Yoshino et al., 2008). For the hydrous minerals, only Guo and Yoshino (2014) measured the pressure effect on the conductivity of brucite. Figure 9 shows the electrical conductivity of the single-crystal brucite as functions of pressure and temperature. Electrical conductivity of the single-crystal brucite increased by 2 orders of magnitude during compression from 3.7 to 13 GPa, irrespective of crystallographic direction. However, the pressure effect was very different at pressures lower and higher than 11 GPa. The activation volumes parallel and perpendicular to the *c*-axis are −2.58±0.1 and −2.11±0.14 cm^3/mole at pressures lower than 11 GPa, respectively, whereas, the activation volumes parallel and perpendicular to the *c*-axis are −0.64±0.08 and 0±0.06 cm^3/mole in the pressure range of 11 to 13 GPa, respectively.

Pressure effect on the conductivity of brucite is closely related to the pressure effect on the interaction between neighboring atoms. Neutron diffraction studies (Parise et al., 1994; Catti et al., 1995) have indicated that H atoms (H_1) are disordered off the threefold axis by compression. H can move easily from 6*i* position to H_1' by overcoming the tilt energy of 0.01 eV (Matsushita, 2001) which position is closer to the oxygen (O′) in the neighboring layer. Vacancy in the position of H_2' is necessary for proton migration from H_1' to H_2' (Figure 10). The O⋯O distance will be significantly shortened by compression, which lowers the potential barrier for proton migration (Martens and Freund, 1976). As a result, proton migration becomes easier with increasing pressure. Therefore, the conductivity of brucite increases with pressure. The study of the infrared spectroscopy of brucite (Shinoda et al., 2002) shows that there is a broad absorption band at pressures over 3 GPa and temperature higher than 493 K. The broad absorption band may suggest that free protons occur in brucite and the proton conduction between neighboring layers will be enhanced under high temperature and high pressure. However, the compression between neighboring layers tends to cease when pressure approaches 10 GPa because the compression of brucite becomes isotropic. The dominant compression mechanism changes from interlayer space compression to [MgO_6] octahedral compression at pressures higher than 10 GPa (Nagai et al., 2000). Furthermore, the pressure effect on the diffusivity of proton in brucite is very consistent with the pressure effect on the conductivity of brucite.

Pressure effect on the conductivity of the hydrous silicates with layered structure (e.g., antigorite, talc and DHMS phases, etc.) may be much weaker than that of brucite. Proton exchange between two neighboring hydrogen layers in brucite is much easier than proton migration in silicates with layered structure because they have no face to face hydrogen layers. The compression rate perpendicular to the *c*-axis of silicate minerals (such as antigorite) is much lower

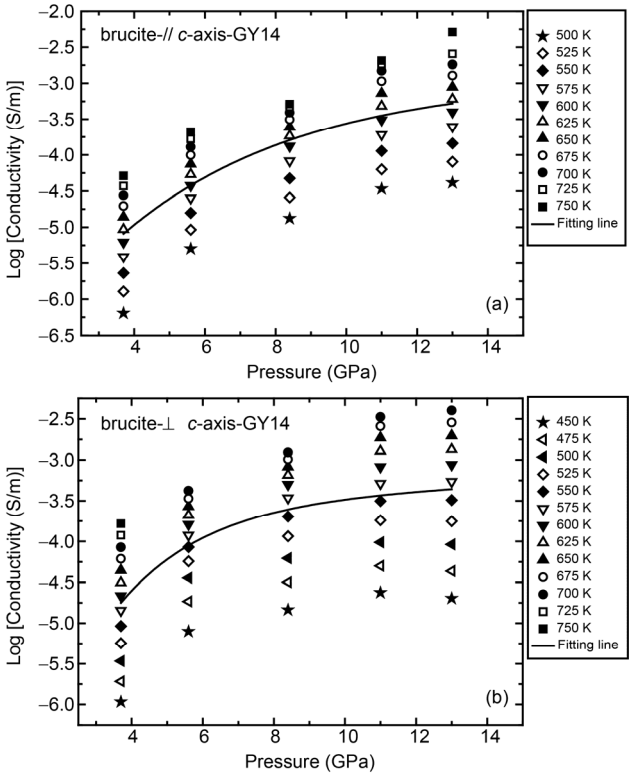

Figure 9 Pressure effect on the electrical conductivity of single-crystal brucite. (a) along *c*-axis; (b) perpendicular to *c*-axis. GY14, Guo and Yoshino (2014).

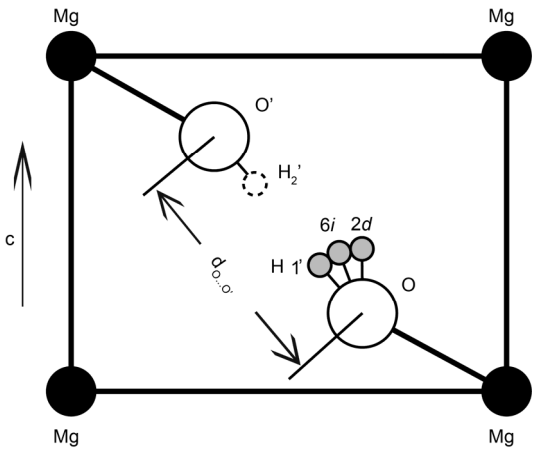

Figure 10 The (110) section of the unit cell of brucite. 2*d* and 6*i* are Wyckoff sites. The jump path is minimized when a proton tilts to the H1' position. $d_{O\cdots O'}$ indicates the interlayer oxygen distance. Modified from Noguchi and Shinoda (2010).

than that along the *c*-axis (Capitani and Stixrude, 2012). Therefore, pressure effect on the conductivity of the hydrous silicate minerals is not strong because the protons prefer to migrate along the hydrogen layer ([MgO_6] layer). For hydrous silicates, the lattice distortion of the hydrogen-bearing octahedral or tetrahedral layers may instead hinder the proton migration, leading to the reduction of the conductivity. Further experiments are needed to demonstrate this mechanism.

7. Geological application: 1-D conductivity-depth profile of the subduction zone

The proportion of the hydrous minerals in the subducting slab may reach 19 vol% in the depth of the transition zone based on the compositional model of Ohtani et al. (2004). Electrical conductivity of the hydrous minerals is higher than that of the NAMs (Guo and Yoshino, 2013). Therefore, the contribution of the hydrous minerals to the electrical profile of the subduction zone must be considered.

Ichiki et al. (2001) reported a 1-D electrical conductivity-depth profile beneath NE China, which showed that the conductivity at the bottom of the transition zone was distinctly high (Figure 11). The origin of the high conductive layer in the transition zone deserves people's attention. A lot of seismic data indicate that the Pacific plate becomes stagnant at the bottom of the transition zone beneath the northeastern China and Philippine Sea (Fukao et al., 2001; Huang and Zhao, 2006). Is the high conductive layer related to the stagnant Pacific slab? To solve this question we should build an electrical conductivity-depth profile of the subduction zone based on the experimental data.

Guo and Yoshino (2013) first calculated the conductivity-depth profile of the cold subduction zone based on the conductivity data of the major minerals, the geothermal data of Peacock (1990) and compositional model (Ohtani et al., 2004). Figure 11 shows the comparison between the 1-D electrical conductivity-depth profiles, the geophysical observations in the subduction zone beneath northeastern China and Philippine Sea and the MT data of the global average. However, the Hashin-Shtrikman (HS) upper bound is far below the geophysical observations, suggesting that a "dry" (fluid-free) and cold subducting slab cannot account for the high conductive layer in the transition zone beneath NE China and Philippine Sea. Thermal structure of the stagnant Pacific slab at the the transition zone depth should be higher than a typical cold subducting slab because the stagnant slab is likely heated by the surrounding hot rocks during its long-term stagnancy. Geophysical observations indicate that the Pacific slab was accumulated beneath NE China for a long time (ca. 100–140 Myr, Zhao et al., 2009). In this scenario water will be continuously released from the

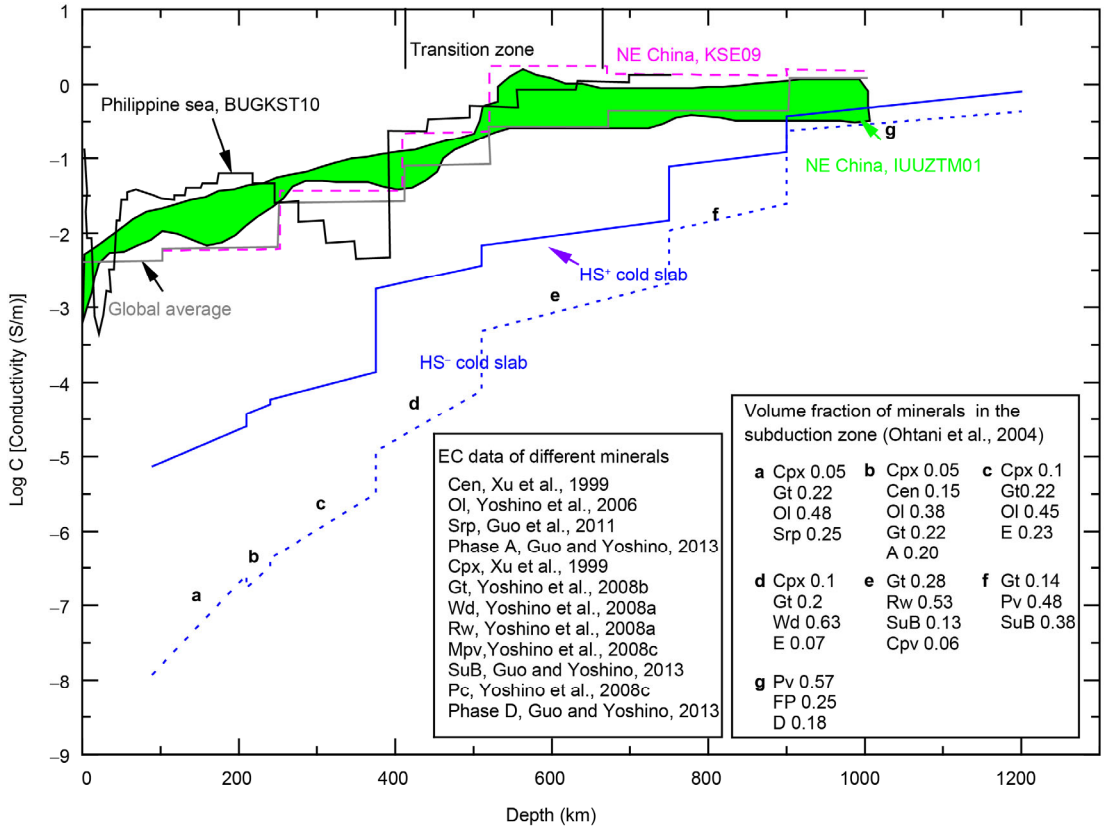

Figure 11 Comparison between the 1-D electrical conductivity-depth profiles and the geophysical observations in the subduction. Modified from Guo and Yoshino (2013).

hydrous minerals through partial or complete dehydration and would therefore enhances the bulk conductivity. Water released from the stagnant slab will move upward to the top of the transition zone due to infiltration and diffusion mechanisms, causing partial melting in the upper mantle (Litasov and Ohtani, 2002). This is consistent with a big mantle wedge model (Zhao et al., 2009), which explains the intraplate volcano in NE China. Pearson et al. (2014) recently reported natural hydrous ringwoodite inclusion (containing 1.5 wt% water) in a diamond. The water-rich nature of this inclusion is direct evidence to show that, at least locally, the transition zone is hydrated, which ends the longstanding controversy about water-rich transition zone (Huang et al., 2005; Yoshino et al., 2008; Green et al., 2010). The hydrous transition zone is directly related to the incorporation of the dehydrated water from the subducting slab into the major minerals of the transition zone. Given that the early Earth itself contains a large amount of hydrogen and in the long-term cooling history of the Earth hydrogen has been incorporated in the major minerals of the transition zone through the gravitational segregation, the transition zone finally will lose water through degassing and dehydrating process if there is no water injection into the transition zone by the subducting slab. The water-rich condition of the transition zone is the consequence of the dynamic balance between the degassing and dehydrating of the mantle and the injection of water into the transition zone by subducting slab. Therefore, the dehydration model of the subducting slab at the depth of the transition zone well explicates the hydrous condition and the deep-focus earthquakes in the transition zone.

8. Conclusion and prospect

In the past decade the conductivity experiments focused on the major minerals of the crust and the mantle; however, experimental studies on hydrous minerals (minor phases) remained scarce. Major issues come out from previous work:

(1) The data reported by different groups are not consistent. The differences may be caused by the experimental conditions, sample container and the different preprocessing of the starting materials.

(2) Investigations on the conduction mechanisms of hydrous minerals are weak. It is still impossible to quantitatively determine the relationship between the conductivity and the hydrogen concentration.

(3) The correlation among different disciplines is not enough to precisely explain the problematic issues. To solve these problems we should synthesize the proofs of petrology, mineralogy, geochemistry, geophysics, etc. The inconsistency of the conductivity reported by different groups should be first clarified in the future studies. For example, we should repeat the experiments by using the same starting material and varying the sample container. Secondly, we should encourage further studies of the conductivity of hydrous minerals such as lawsonite, phengite, chlorite, amphibole. Thirdly, it is necessary to carry out experimental studies about the pressure effect on the conductivity of the silicates with layered structure in order to further help to understand the conduction mechanism of the hydrous minerals. Next, diamond anvil cell experiments combined with *in situ* IR technique would allow us to test the possible partial dehydration phenomena of the hydrous minerals. Finally, electrical conductivity of free-water bearing system, hydrous minerals and NAMs in the close system condition should be measured to better constrain the origin of the high conductivity anomalies in the transition zone.

Acknowledgements *I thank the two anonymous reviewers for their constructive comments which greatly enhanced the manuscript. I also thank Vincent Soustelle for his help in polishing the language. This study was supported by the National Natural Science Foundation of China (Grant Nos. 41590623 & 41472040), the Fundamental Research Funds for the Central Universities, China University of Geosciences (Grant No. CUGL150801) and Special Fund from the State Key Laboratory of Geological Processes and Mineral Resources, China University of Geosciences (Grant No. MSFGPMR201408).*

References

Capitani G C, Stixrude L. 2012. A first-principle investigation of antigorite up to 30 GPa: Structure behavior under compression. Am Mineral, 97: 1177–1186

Catti M, Ferraris G, Hull S, Pavese A. 1995. Static compression and H disorder in brucite, $Mg(OH)_2$, to 11 GPa: A powder Neutron diffraction study. Phys Chem Miner, 22: 200–206

Freund F, Wengeler H. 1980. Proton conductivity of simple ionic hydroxides. Part I: The proton conductivities of $Al(OH)_3$, $Ca(OH)_2$ and $Mg(OH)_2$. BerBunsenges Phys Chem, 84: 866–873

Fuji-ta K, Katsura T, Matsuzaki T, Ichiki M. 2007. Electrical conductivity measurements of brucite under crustal pressure and temperature conditions. Earth Planets Space, 59: 645–648

Fukao Y, Widiyantoro S, Obayashi M. 2001. Stagnant slabs in the upper and lower mantle transition region. Rev Geophys, 39: 291–323

Gasc J, Brunet R, Bagdassarov N, Morales-Flórez V. 2011. Electrical conductivity of polycrystalline $Mg(OH)_2$ at 2 GPa: Effect of grain boundary hydration-dehydration. Phys Chem Miner, 38: 543–556

Green II H W, Chen W, Brudzinski M R. 2010. Seismic evidence of negligible water carried below 400-km depth in subducting lithosphere. Nature, 467: 828–831

Guo X, Yoshino T, Katayama I. 2011. Electrical conductivity anisotropy of deformed talc rocks and serpentinites at 3 GPa. Phys Earth Planet Inter, 188: 69–81

Guo X, Yoshino T, Okuchi T, Tomioka N. 2013. H-D interdiffusion in brucite at pressures up to 15 GPa. Am Mineral, 98: 1919–1929

Guo X, Yoshino T. 2013. Electrical conductivity of dense hydrous magnesium silicates with implication for conductivity in the stagnant slab. Earth Planet Sci Lett, 369–370: 239–247

Guo X, Yoshino T.2014. Pressure-induced enhancement of proton conduction in brucite. Geophys Res Lett, 41: 813–819

Hinze E, Will G, Cemic L. 1981. Electrical conductivity measurements on synthetic olivines and on olivine, enstatite and diopside from Dreiser Weiher, Eifel (Germany) under defined thermodynamic activities as a function of temperature and pressure. Phys Earth Planet Inter, 25: 245–254

Huang J, Zhao D. 2006. High-resolution mantle tomography of China and

surrounding regions. J Geophys Res, 111: B09305, doi: 10.1029/2005JB004066
Huang X, Xu Y, Karato S. 2005. Water content in the transition zone from electrical conductivity of wadsleyite and ringwoodite. Nature, 434: 746–749
Ichiki M, Uyeshima M, Utada H. 2001. Upper mantle conductivity structure of the back-arc region beneath northeastern China. Geophys Res Lett, 28: 3773–3776
Karato S. 1990. The role of hydrogen in the electrical conductivity of the upper mantle. Nature, 347: 273–274
Katayama I, Hirauchi K, Michibayashi K, Ando J. 2009. Trench-parallel anisotropy produced by serpentine deformation in the hydrated mantle wedge. Nature, 461: 1114–1117
Katsura T, Sato K, Ito E. 1998. Electrical conductivity of silicate perovskite at lower-mantle conditions. Nature, 395: 493–495
Kawano S, Yoshino T, Katayama I. 2012. Electrical conductivity of magnetite-bearing serpentinite during shear deformation. Geophys Res Lett, 39: L20313, doi: 10.1029/2012GL053652
Kurtz R D, DeLaurier, J M, Gupta J C. 1986. A magnetotelluric sounding across Vancouver Island detects the subducting Juan de Fuca plate. Nature, 321: 596–599
Litasov K D, Ohtani E. 2002. Phase relations and melt compositions in CMAS-pyrolite-H_2O systems up to 25 GPa. Phys Earth Planet Inter, 134: 105–127
Martens R, Freund F. 1976. The potential energy curve of the proton and dissociation energy of the OH^{-1} ion in $Mg(OH)_2$. Phys Status Solid A-Appl Mat, 37: 97–104
Matsushita E. 2001. Tunneling mechanism on proton conduction in perovskite oxides. Solid State Ion, 145: 445–450
Meade C, Jeanloz R. 1991. Deep-focus earthquakes and recycling of water into the Earth's mantle. Science, 252: 68–72
Mei S, Kohlstedt D L. 2000. Influence of water on plastic deformation of olivine aggregates 1. Diffusion creep regime. J Geophys Res, 105: 21457–21469
Nagai T, Hattori T, Yamanaka T. 2000. Compression mechanism of brucite: An investigation by structural refinement under pressure. Am Mineral, 85: 760–764
Nishi M, Irifune T, Tsuchiya J, Tange Y, Nishihara Y, Fujino K, Higo Y. 2014. Stability of hydrous silicate at high pressures and water transport to the deep lower mantle. Nat Geosci, 7: 224–227
Nishihara Y, Shinmei T, Karato S. 2006. Grain-growth kinetics in wadsleyite: Effects of chemical environment. Phys Earth Planet Inter, 154: 30–43
Noguchi N, Shinoda K. 2010. Proton migration in portlandite inferred from activation energy of self-diffusion and potential energy curve of OH bond. Phys Chem Minerals, 37: 361–370
Ohtani E, Amaike Y, Kamada S, Sakamaki T, Hirao N. 2014. Stability of hydrous phase H $MgSiO_4H_2$ under lower mantle conditions. Geophys Res Lett, 41, doi: 10.1002/2014GL061690
Ohtani E, Litasov K, Hosoya T, Kubo T, Kondo T. 2004. Water transport into the deep mantle and formation of a hydrous transition zone. Phys Earth Planet Inter, 143–144: 255–269
Parise J, Leinenweber K, Weidner D, Tan K. 1994. Pressure-induced H bonding: Neutron diffraction study of brucite, Mg(OD)2 to 9.3 GPa. Am Mineral, 79: 193–196
Pawley A R, Holloway J R. 1993. Water sources for subduction zone volcanism: New experimental constraints. Science, 260: 664–667
Peacock S M. 1990. Fluid processes in subduction zone. Science, 248: 329–337
Pearson D G, Brenker F E, Nestola F, McNeill J, Nasdala L, Hutchison M T, Matveev S, Mather K, Silversmit G, Schmitz S, Vekemans B, Vincze L. 2014. Hydrous mantle transition zone indicated by ringwoodite included within diamond. Nature, 507: 221–224
Reynard B, Mibe K, Van de Moortele B. 2011. Electrical conductivity of the serpentinised mantle and fluid flow in subduction zones. Earth Planet SciLett, 307: 387–394
Schramke J A, Kerrick D M, Blencoe J G. 1982. Experimental determination of the brucite=periclase+water equilibrium with a new volumetric technique. Am Mineral, 67: 269–276
Shinoda K, Yamakata M, Nanba T, Kimura H, Moriwaki T, Kondo Y, Kawamoto T, Niimi N, Miyoshi N, Aikawa N. 2002. High-pressure phase transition and behavior of protons in brucite $Mg(OH)_2$: A high-pressure-temperature study using IR synchrotron radiation. Phys Chem Miner, 29: 396–402
Ulmer P, Trommsdorff V. 1995. Serpentine stability to mantle depths and subduction-related magmatism. Science, 268: 858–861
Wanamaker P E, Caldwell T G, Jiracek G R, Maris V, Hill G J, Ogawa Y, Bibby H M, Bennie S L, Heise W. 2009. Fluid and deformation regime of an advancing subduction system at Marlborough, New Zealand. Nature, 460: 733–737
Wang D, Karato S. 2013. Electrical conductivity of talc aggregates at 0.5 GPa: Influence of dehydration. Phys Chem Minerals, 40: 11–17
Winkler K W, Nur A. 1982. Seismic attenuation: Effects of pore fluids and frictional-sliding. Geophysics, 47: 1–15
Xu Y, Shankland T J, Duba A G. 2000. Pressure effect on electrical conductivity of mantle olivine. Phys Earth Planet Inter, 118: 149–161
Yang X. 2014. Electrical petrology: Principles, methods and advances (in Chinese). Sci Sin Terrae, 44: 1884–1990
Yoshino T, Manthilake G, Matsuzaki T, Katsura T. 2008. Dry mantle transition zone inferred from the conductivity of wadsleyite and ringwoodite. Nature, 451: 326–329
Yoshino T, Matsuzaki T, Yamashita S, Katsura T. 2006. Hydrous olivine unable to account for conductivity anomaly at the top of the asthenosphere. Nature, 443: 973–976
Yoshino T. 2010. Laboratory electrical conductivity measurements of mantle minerals. Surv Geophys, 31: 163–206
Zhao D, Tian Y, Lei J, Liu L, Zheng S. 2009. Seismic image and origin of the Changbai intraplate volcano in East Asia: Role of big mantle wedge above the stagnant Pacific slab. Phys Earth Planet Inter, 173: 197–206
Zhu M, Xie H, Guo J, Bai W, Wu Z. 2001a. Impedance spectroscopy analysis on electrical properties of serpentine at high pressure and high temperature. Sci China Ser D-Earth Sci, 44: 336–345
Zhu M, Xie H, Guo J, Xu Z. 2001b. An experimental study on electrical conductivity of talc at high temperature and high pressure. Chin J Geophys, 44: 427–434